

1 **Numerical Investigation of the Middle Atlantic Bight Shelfbreak**
2 **Frontal Circulation Using a High-resolution Ocean Hindcast Model**

3 Ke Chen and Ruoying He*

4 Department of Marine, Earth and Atmospheric Sciences

5 North Carolina State University

6

7 March 15, 2009

8 submitted to *Journal of Physical Oceanography*

9 * Corresponding author: Dr. Ruoying He, Tel: 919-513-0249; Email: rhe@ncsu.edu

10

11 **Abstract**

12 A nested high-resolution ocean model is used to hindcast the Middle Atlantic Bight
13 (MAB) shelfbreak circulation from December 2003 to June 2008. The model is driven by tidal
14 harmonics, realistic atmospheric forcing, and dynamically consistent initial and open boundary
15 conditions obtained from the large-scale circulation model. Simulated shelfbreak sea levels and
16 tracer fields compare favorably with satellite observations and in-situ hydrographic climatology,
17 demonstrating the utility of this nested ocean model for resolving the MAB shelfbreak
18 circulation. The resulting time and space continuous hindcast solutions between January, 2004
19 and December, 2007 are used to describe the mean structures and temporal variations of the
20 shelfbreak front and jet, the bottom boundary layer detachment, and the migrations of the
21 shelfbreak front. It is found that the shelfbreak jet and boundary convergence reach their largest
22 intensities in the spring season, at which time the foot of the front also migrates to its farthest
23 offshore position. Vorticity and momentum analyses reveal that the magnitude ratio of the mean

24 relative vorticity is about 2:1 between the seaward and the shoreward portions of the shelfbreak
25 front. The shelfbreak ageostrophic circulation is largely controlled by the viscosity in the
26 boundary layers and by the nonlinear advection in the flow interior. Simulated three-dimensional
27 velocity and tracer fields are used to estimate the transport, heat and salt fluxes across the 200-m
28 isobath. Within the model domain, the total cross-shelf water transport, the total heat flux and
29 the total salt flux are 0.035 ± 0.26 sv, $1.0 \times 10^3 \pm 1.43 \times 10^4$ W / m²,
30 $6.67 \times 10^{-5} \pm 6.98 \times 10^{-4}$ Kg / m²s, respectively. Based on the 4-yr of shelfbreak circulation
31 hindcast, the Empirical Orthogonal Function (EOF) analysis is applied to identify dominant
32 modes of the shelfbreak current. The first EOF mode accounts for 61% variance, confirming that
33 the shelfbreak jet is a persistent year-round circulation feature. The second mode accounts for
34 13% variance, representing baroclinic eddy passages across the shelfbreak.

35

36 **1. Introduction**

37 The shelfbreak front in the Middle Atlantic Bight (MAB) is the water mass boundary
38 between the cold, fresh water on the MAB shelf and the warm, saline water of the Slope Sea.
39 Associated with the front is a narrow shelfbreak jet, which has been estimated to transport
40 approximately 0.2-0.3 sv of water equator-ward south of the New England (*Linder and*
41 *Gawarkiewicz, 1998*). This shelfbreak frontal jet is a part of the large-scale buoyancy driven
42 coastal current system that originates from the Labrador Sea (*Chapman and Beardsley, 1989*;
43 *Loder et al, 1998*). It exerts strong influence on the coastal environment in the northwest
44 Atlantic, impacting cross-shelf exchanges of mass, heat, salt, the dispersion of coastal
45 contaminants, and the nutrient supply to coastal ecosystems. For example, the shelfbreak front
46 and jet are found to be important for many commercial fisheries because of the enhanced

47 primary productivity associated with the front (e.g., *Marra et al.*, 1982, 1990; *Ryan et al.*, 1999a,
48 1999b).

49 Understanding the shelfbreak frontal dynamics has been the major topic of numerous
50 earlier studies. Hydrographic surveys by *Beardsley and Flagg* (1976) and *Burrage and Garvine*
51 (1988) provided synoptic snapshots that generally describe the thermocline structure of the front.
52 Long-term mooring arrays, such as the Nantucket Shoals Flux Experiment (NSFE) (*Beardsley et*
53 *al.*, 1985), the Shelf Edge Exchange Process (SEEP) Experiment (*Aikman et al.*, 1988; *Houghton*
54 *et al.*, 1988) and SEEP II Experiment (*Houghton et al.*, 1994; *Flagg et al.*, 1994) addressed the
55 long-term statistics of the velocity and temperature structure of the front. By area-averaging
56 long-term hydrographic data, *Linder and Gawarkiewicz* (1998) offered climatological mean
57 conditions of MAB shelfbreak frontal structures, the migration of the front bottom foot, and the
58 associated geostrophic velocity fields. More recently, *Fratantoni et al.* (2001) studied the
59 structure of shelfbreak jet based on two-year (1995 -1997) ADCP surveys. While providing
60 many valuable insights on the shelfbreak frontal dynamics, these studies are still limited by
61 temporal and spatial resolutions and subjected to the question how representative they are. In
62 particular, work including *Garvine et al.*, (1988), *Lozier et al.*, (2002) and *Gawarkiewicz et al.*
63 (2004) showed that frontal instabilities and shelf-slope interactions are reoccurring features with
64 fine temporal and spatial scales as small as 1-2 day and 8-15km, respectively. Improved
65 understanding of the MAB shelfbreak circulation and better quantification of its variations
66 therefore require high-resolution, space and time continuous realizations of ocean state variables,
67 from which detailed dynamics can be gleaned.

68 In this study, we approach this problem through a realistic, high-resolution circulation
69 hindcast experiment. We start in Section 2 with the description of the shelfbreak ocean model

70 utilized in this research. Section 3 presents model-data comparisons, the structures of simulated
71 mean shelfbreak front and jet, and their temporal variations. More in-depth circulation dynamical
72 analysis and cross-shelf transport and flux estimates are provided in Section 4, followed by the
73 discussion and summary in Section 5.

74

75 **2. Model**

76 Our high resolution shelfbreak simulation was performed with the Regional Ocean
77 Modeling System (ROMS), a free-surface, hydrostatic, primitive-equation model. ROMS
78 employs split-explicit separation of fast barotropic and slow baroclinic modes, and is formulated
79 in vertically stretched terrain-following coordinates using algorithms described in details by
80 *Shchepetkin and McWilliams* (2005). The ROMS computational kernel includes high-order
81 advection and time-stepping schemes, weighted temporal averaging of the barotropic mode to
82 reduce aliasing into the slow baroclinic motions, and conservative parabolic splines for vertical
83 discretization. A redefinition of the barotropic pressure-gradient term is also applied in ROMS to
84 reduce the pressure-gradient truncation error, which has previously limited the accuracy of
85 terrain-following coordinate models.

86 The model domain encompasses the shelfbreak regions offshore of Nantucket shoals in
87 the northeast and Hudson Canyon in the southwest (**Figure 1**). The model horizontal resolution
88 is 1 km. Vertically, there are 36 terrain-following levels in the water column with higher
89 resolution near the surface and bottom to better resolve ocean boundary layers.

90

91 **2.1. Open boundary and Initial Conditions**

92 To specify open boundary conditions for this shelfbreak model, we nested it inside the
93 MABGOM ROMS described and validated by *He and Chen* (submitted). The MABGOM model
94 itself was nested in the global circulation simulation provided by HyCOM/NCODA (Hybrid
95 Coordinate Ocean Model together with NRL Coupled Ocean Data Assimilation scheme,
96 *Chassignet et al.*, 2006). A one-way nesting approach was adopted in this setup to connect the
97 ‘parent model’ with the ‘child model’. Specifically, open boundary conditions (OBCs) was
98 applied to tracers and baroclinic velocity following the method of *Marchesiello et al.* (2001),
99 whereby Orlanski-type radiation conditions were used in conjunction with relaxation (with
100 timescale of 0.5 days on inflow and 10 days on outflow) to MABGOM solutions. Free surface
101 and depth-averaged velocity boundary conditions were specified using the method of *Flather*
102 (1976) with the external subtidal values defined by MABGOM, plus M_2 tidal harmonics from an
103 ADCIRC tidal simulation of the western Atlantic (*Luettich et al.* 1992). The latter M_2
104 information provides needed tidal mixing, which is an important element of the regional
105 circulation. We applied the method of *Mellor and Yamada* (1982) to compute vertical turbulent
106 mixing, as well as the quadratic drag formulation for the bottom friction specification. Major
107 advantages of such nesting configuration include: 1) it allows to the “child model” to account for
108 the upstream and deep-ocean forcing in a dynamically consistent and quantitatively accurate
109 manner; and 2) the higher resolution enables the shelfbreak ROMS to better resolve the frontal
110 circulation underpinned in this research.

111

112 **2.2. Surface Forcing**

113 We utilized surface forcing from NOAA NCEP North America Regional Reanalysis
114 (NARR), which has the spatial and temporal resolutions of 35-km and 3 hourly, respectively.

115 Air-sea fluxes of momentum and buoyancy were computed by applying the standard bulk
116 formulae (Fairall *et al.* 2003) to NARR marine boundary-layer winds, air temperature, relative
117 humidity, air pressure, along with ROMS generated surface current. To further constrain the
118 spatial pattern of the net surface heat flux, we implemented a thermal relaxation term following
119 He and Weisberg (2002), such that

$$120 \quad K_H \frac{\partial T}{\partial Z} = \frac{Q}{\rho C_p} + c(T_{obs} - T_{mod}) \quad (1)$$

121 where $c = 0.5 \text{ day}^{-1}$, and T_{obs} is the daily, 10-km resolution blended cloud-free surface
122 temperature field generated by NOAA Coast Watch.

123 We started the shelfbreak ROMS hindcasts on December, 2003 and ran the model
124 continuously till June, 2008. Initial conditions for the shelfbreak circulation simulations were
125 taken from the MABGOM ROMS simulation on December 1st, 2003.

126

127 **3. Results**

128 Standard circulation state variables (sea level, currents, temperature, and salinity) were
129 archived at daily interval for the 4.5 year of hindcast period. For model validations and analyses
130 described below, we concentrated on the simulation over the period of 4 full years spanning from
131 January 1, 2004 to December 31, 2007. Limited by scarce shelfbreak in-situ observations, we
132 used satellite observations and hydrographic climatology to gauge the model's performance.

133

134 **3.1. Model Data Comparisons**

135 *A. Sea Surface height comparisons*

136 Satellite altimeter data provide a useful means to examine the model's skill in
137 reproducing sea surface height distribution. For the model validation purpose, we obtained
138 $1/3^\circ \times 1/3^\circ$ along-track SSHA product from French Archiving, Validation of Satellite
139 Oceanographic Data [AVISO] (*Rio and Hernandez, 2004*) for the MAB shelfbreak region. There
140 are three satellite tracks inside the model domain. Among them, we focus on a cross-shelf track
141 that is nearly aligned with the earlier PRIMER cross-section (*Fratantoni et al., 2001*). Given that
142 the along-track satellite data are only available every 9 days; we sampled our simulated subtidal
143 sea surface height anomaly (SSHA) at the same time when altimeter observations were available.

144 The Hovmoller diagram of observed SSHA shows the sea levels along this cross-shelf
145 transect are the highest (lowest) during the fall (spring) season (**Figure2**). Throughout the
146 examining period, the absolute surface height variation is up to 0.25 m, which is contributed by
147 the combined effects of surface heating and horizontal advection. Such sea level responses were
148 generally simulated correctly by the shelfbreak model. While the model is missing some of the
149 fine-scale sea level structures, it captures the seasonal and interannual variability reasonably well.
150 Statistically speaking, the overall correlation coefficient between simulated and observed SSHA
151 is 0.53 with the 95% confidence level.

152

153 ***B. Shelfbreak hydrography comparisons***

154 We next sampled mean temperature and salinity along the Nantucket transect (Figure 1)
155 and compared these tracer fields with early climatology averaged by *Linder and Gawarkiewicz*
156 (1998) for the similar segment of the MAB shelfbreak. The Nantucket transect is nearly
157 perpendicular to the local isobath, so the choice of this transect also allows for direct
158 examinations of the shelfbreak jet and its along-shelf transport. To be consistent with *Linder and*

159 *Gawarkiewicz* climatology, simulated based bi-monthly mean temperature and salinity fields
160 were produced from the 4-year hindcast solutions.

161 The bimonthly temperature fields (**Figure 3**) exhibit strong seasonal variability. During
162 winter months (December to March), surface cooling together with enhanced mixing induced by
163 convective overturning and storm events keep shelf waters weakly stratified, as shown by both
164 model and observation. The thermocline starts to develop as the season progresses. By the spring
165 to summer time (April to July), a strong thermocline has established, separating the warm upper
166 layer from the cold bottom water. The latter becomes the so called MAB “cold pool”, as
167 described by *Beardsley and Flag*, (1976) and *Houghton et al.*, (1982) among other studies.
168 Further offshore, both observation and simulation show an abrupt horizontal temperature
169 gradient at the shelfbreak, known as the “shelfbreak front”. In fall (August-November), the shelf
170 waters transition from vertically stratified to horizontally stratified. As a result, the shelfbreak
171 temperature front becomes less pronounced by this time compared to its spring and summer
172 conditions. The bimonthly salinity fields (**Figure 4**) exhibit relatively weaker seasonal variability.
173 Unlike the temperature, both the simulation and observation show the shelfbreak salinity front is
174 a persistent feature throughout the year, with a gradient of ~1-2 psu change over a distance of 10-
175 20km. We note the *Linder and Gawarkiewicz* climatology was resulted from a time and space
176 averaging of hydrographic data collected in the vicinity of MAB shelfbreak in nearly 100 years,
177 whereas the model results reported here are based on the 4-year shelfbreak circulation hindcast.
178 Albeit differences in the time span, and the temporal and spatial resolutions between the model
179 fields and climatology, it is encouraging to see this shelfbreak ROMS is capable of reproducing
180 essential features of shelfbreak temperature and salinity fields, and their respective seasonal

181 evolutions. These general agreements verify the model's utility for resolving shelfbreak
182 circulation, lending confidence of using its hindcast solutions for detailed dynamic analysis.

183

184 **3.2. Model Analysis**

185 We next use the high-resolution, space and time continuous hindcast solutions to
186 characterize the MAB shelfbreak jet and frontal structures along the Nantucket transect.

187

188 ***A. Mean shelfbreak frontal structures***

189 First we concentrated on the structures of mean temperature, salinity, along and across-
190 shelf velocity fields (**Figure 5**), each obtained by temporally averaging their respective solutions
191 from January 1st, 2004 to December 31st, 2007.

192 The mean temperature field highlights the co-existence of "cold pool" on the shelf and
193 the temperature front at the shelf break. Within the "cold pool" area, the bottom water is about 4-
194 5 °C cooler than the surface water. At the shelfbreak, the upward tilted temperature front extends
195 to 20-m below the surface. A similar shelfbreak frontal structure is also seen in the mean salinity
196 field. As the salinity front extends all the way to the surface, it has a more clear surface signature
197 than the temperature front.

198 The mean alongshore velocity transect shows the shelfbreak circulation consists of an
199 equator-ward shelfbreak jet and a near bottom polar-ward slope sea current (*Flagg et al, 2006*).
200 The former current moves at 0.1 ms^{-1} , with the majority of its flow trapped within the upper 70-
201 m. Consistent with findings of earlier studies (*Gawarkiewicz, 2004; Fratantoni, 2001*), the jet is
202 located at the shoreward side of the shelfbreak front. If using 100-m and 40-km as the ranges of
203 depth and width for the shelfbreak current, we estimated the simulated along-jet transport is 0.31

204 sv, a value comparable with previous estimates (*Beardsley et al*, 1985; *Linder and Gawarkiewicz*,
205 1998; *Fratantoni*, 2001). The cross-shelf mean velocity exhibits a layered -structure similar to
206 what was discussed by *Lentz* (2008). It has a seaward moving surface flow (the upper 25 m), a
207 shoreward moving interior flow, which is underlaid by another weak seaward moving flow near
208 the bottom. It should be noted that the 4-year temporal averaging may smooth out small-scale
209 frontal structures that may otherwise be observed by the synoptic in-situ surveys. We will
210 examine the small scale variability in a different study.

211

212 ***B. Bimonthly mean shelfbreak jet structures***

213 To quantify the temporal variations of the shelfbreak jet associated with bi-monthly
214 hydrography presented in 3.1, we further computed bi-monthly velocity means with simulated
215 sub-tidal currents (**Figure 6**). In December and January, the shelfbreak jet is surface intensified
216 within a thin (<50 m) but broad (> 20 km) upper layer. The polar-ward slope water current is
217 largely absent at this time of the year. Consequently, the equator-ward shelfbreak currents
218 transport a volume of 0.72 sv to the south, the largest value throughout the year. The shelfbreak
219 jet then weakens in February and March, with the core of jet shifting offshore. This is
220 accompanied by an onshore motion of the slope water current. Transports of these two currents
221 counteract each other, resulting in a net equator-ward transport of only 64% of its winter value.
222 In spring (April – May), the shelfbreak jet gets reinforced with the core of jet confined to within
223 a few km shoreward of the shelfbreak. The jet speed reaches its annual maximum 0.3 ms^{-1} , a
224 value that is consistent with observation of *Fratantoni et al.* (2001). The slope current seaward of
225 the shelfbreak is similarly intensified, but to a less extent. Consequently, the net equator-ward
226 transport is 0.62 sv, the second highest value of the year. Starting in August, the jet begins to

227 weaken with its core going deeper and shoreward. The maximum velocity now reduces to
228 0.1ms^{-1} . These changes are in response to shelf water destratification associated with enhanced
229 cooling and mixing, leading to weakened across-shelf density gradient (e.g., Figure 3). By
230 October and November, the shelfbreak jet structure becomes less clear. Counteracted by the
231 enhanced polar-ward slope current, the net equator-ward transport now reaches its minimum
232 value of the year.

233

234 *C. Bimonthly mean bottom boundary layer detachment*

235 An important feature of the MAB shelfbreak circulation is the convergent flow near the
236 bottom of the shelfbreak front and its related bottom boundary layer (BBL) detachment process
237 (*Gawarkiewicz and Chapman, 1992; Chapman and Lentz, 1994; Barth et al., 1998; Pickart et al.,*
238 *2000; Linder and Gawarkiewicz, 2004*). *Pickart et al. (200)* showed a useful means to quantify
239 such BBL detachment is through the Accumulated Property Change (APC) calculation. The
240 basic idea is that upwelling along the isopycnal layer in which the detachment is occurring
241 should result in a weaker water property. Hence by computing the accumulated temperature
242 change (ATC) along tilted isopycnals in a cross front transect and tracking tongues of low ATC,
243 one can assess the intensity of bottom boundary layer detachment. Following this idea, we
244 computed density and its associated ATC using bimonthly temperature and salinity fields. The
245 resulting bi-monthly shelfbreak ATC fields (**Figure 7**) indicate the bottom convergence is indeed
246 a discernable feature in the winter, spring, and summer seasons with its intensity seemingly
247 proportional to the degree of isopycnal tilting, i.e., more BBL convergence occurs when the
248 isopycnals are more upward tilted at the shelfbreak. No significant ATC tongue structure is
249 identified in fall when isopycnals are relatively flat, suggesting a shutdown of the BBL

250 convergence. We note findings here are consistent with *Linder and Gawarkiewicz* (2004) BBL
251 discussion. One caveat is that the present ATC calculations are based on the bimonthly mean
252 tracer fields. A more rigorous quantification of the BBL detachment and shelfbreak upwelling
253 rate estimation would require a focused case study using instantaneous 3-dimensional tracer and
254 circulation fields. This is an ongoing effort that we will report in a future correspondence.

255

256 *D. Cross-shelf migration of shelfbreak front*

257 Following *Beardsley and Flagg* (1976) and *Linder and Gawarkiewicz* (1998), we next
258 used the 34.5 psu isohaline to define the front boundary and investigate spatial variations of the
259 foot of the front (left panel, **Figure 8**). The 34.5 psu isohaline is generally tilted upward.
260 Consistent with our earlier discussion, the largest tilting angle occurs in the spring season, when
261 the maximum speed of baroclinic shelfbreak jet occurs. Throughout the year, the monthly mean
262 foot position migrates between 100-m and 160-m isobaths, which translates into a horizontal
263 displacement of 15~20 km. In terms of the water depth of the frontal foot, the monthly position
264 histogram (right panel, **Figure 8**) indicates the front moves to its farthest onshore position in the
265 winter (November and December), and its farthest offshore position in the spring (April and
266 May), respectively. Consistent with finding of *Linder and Gawarkiewicz* (1998), results here
267 suggest that systematic in-situ samplings of the shelf break front would require a wide spatial
268 coverage to resolve variations of the front.

269

270 **4. Discussion**

271 *A. Vorticity and momentum balance*

272 Based on the mean shelfbreak circulation fields, we can compute the relative vorticity
273 $\frac{\partial v}{\partial x} - \frac{\partial u}{\partial y}$ along the Nantucket transect (left panel, **Figure 9**) The resulting mean vorticity field
274 after scaled by the local Coriolis parameter gives the Rossby number $R_o = \zeta / f$. Seaward of the
275 shelfbreak jet, R_o is positive with a value of 0.15. Shoreward of the jet, R_o is negative with a
276 value approaching -0.07. The result here compares favorably with the observational based
277 vorticity calculation reported by *Fratantoni et al.* (2001) [right panel, **Figure 9**]. It is also in
278 agreement with *Gawarkiewicz et al.* (2001) showing the absolute ratio of relative vorticity is
279 about 2:1 between the seaward and the shoreward portions of the front. Further examinations of
280 the mean shelfbreak circulation (Figure 5) indicate the presence of polar-ward slope water
281 current induces a large velocity shear, contributing to a stronger cyclonic circulation seaward of
282 the shelfbreak. The consistency between observed and simulated vorticity fields further confirms
283 that the shelfbreak model captures the essence of shelfbreak circulation dynamics.

284 Term-by-term momentum analysis offers additional insights on the shelfbreak circulation.
285 By examining the relative importance of the local rate of change, the Coriolis force, the
286 horizontal pressure gradient force, horizontal and vertical advection terms, and the horizontal and
287 vertical viscosity terms, one can identify key balances dominating the shelfbreak circulation
288 structure. We focus on the mean momentum balance in the cross-shelf direction (**Figure 10**). As
289 expected, both the Coriolis force and pressure gradient force are the leading (an order of
290 magnitude larger than others) terms and together they constitute the geostrophic balance. Indeed,
291 the shelfbreak jet and the polar-ward moving slope current are to the first order geostrophic
292 flows. The residual of Coriolis force plus pressure gradient force leads to the ageostrophic
293 circulation. The ageostrophic momentum is balanced largely by the frictional viscosity in the

294 surface and bottom boundary layers. The residual of those two is further balanced by the
 295 nonlinear advection presented primarily in the flow interior. The sum of ageostrophic momentum,
 296 viscosity and advection terms gives rise to the local rate of change of the mean across-shelf
 297 velocity (last panel in Figure 10), which is of four order-of-magnitudes smaller than the Coriolis
 298 force. In reality, we expect at any given time, the local rate of change of the shelfbreak
 299 circulation would be a significantly large number due to the transit nature of the system (e.g.,
 300 *Lozier et al., 2002*). A large number of snapshots would have to be ensembled to produce a
 301 steady state mean field. The fact that the local rate of change term being very small here
 302 suggests that the temporal averaging of 4-yr of daily model output fields produces a credible
 303 representation of the mean state of the shelfbreak circulation.

304

305 ***B. Cross shelf transport and flux***

306 Quantifying the slope/shelf water mass and flux exchanges has been a longstanding
 307 research problem in the MAB regional oceanography (*Beardsley and Boicourt, 1981; Lord et*
 308 *al., 1998; Lozier et al., 2001; Fratantoni et al., 2001; Gawarkiewicz et al., 2004*). Here, we
 309 approached this problem by using simulated circulation fields. To do that, we followed *He and*
 310 *Chen* (submitted) by selecting the 200m isobath as the shelf-slope boundary and compute the
 311 cross-shelf water mass transport. Simulated 3-d velocity fields were firstly rotated into the
 312 normal and tangential components based on the local orientations of the 200-m isobath. The
 313 resulting normal component of velocity U_N was then integrated with local depth Z and along-
 314 isobath length S to yield the volume transport value according to:

$$315 \quad Q = \int_{-H}^{s_0} \int_{\eta}^{\eta} u_N(s, z) ds dz \quad (2)$$

316 where S_0 is the along-isobath distance. This calculation reveals that across the 200-m isobath
 317 within the shelfbreak model domain, the total cross-shelf transport is 0.035 ± 0.26 sv. It is worth
 318 noting that the standard deviation of such transport is an order of magnitude larger than the mean,
 319 indicating that across-shelfbreak mass exchange is highly variable.

320 The spatial distribution of such variability is examined in **Figure 11**. In general, the mean
 321 transport near the Nantucket Shoal (0-100km along isobath) is weakly onshore. Immediately
 322 downstream (100-200 km), the mean transport becomes weakly offshore with a value of ~ 0.002
 323 sv. The overall variations over these two segments are both relatively small. Transport values
 324 then become highly fluctuating as they approach the Hudson Canyon off New York (200-300
 325 km). Here, the standard deviations range from -0.02 to 0.02 sv, which are presumably related to
 326 active eddy activities often observed in this area.

327 The cross-shelf flux of any quantity ϕ can be estimated by the method proposed by
 328 *Garvine et al. (1988)*, such that

$$329 \quad F(z) = \frac{1}{\Delta z \Delta x} \int_{z-\frac{\Delta z}{2}}^{z+\frac{\Delta z}{2}} \int_{x_1}^{x_2} \Phi(x, z_1) dx dz \quad (3)$$

330 For the heat flux, we defined,

$$331 \quad \Phi = \rho C_p (T - T_m)(v - v_m) \quad (4)$$

332 For the salt flux, we defined:

$$333 \quad \Phi = \frac{\rho}{1000} (S - S_m)(v - v_m) \quad (5)$$

334 where S , T , v are the salinity, temperature and cross-shelf velocity, respectively. The variables
 335 with subscript m indicate the temporal mean values along the 200m isobath within the shelfbreak
 336 model domain. ρ is water density and C_p , the seawater specific heat.

337 We found the 4-yr mean total heat flux is shoreward at $1.0 \times 10^3 \pm 1.43 \times 10^4 W / m^2$,
338 indicating on average the slope sea is acting as the source of heat for the shelf waters. Depending
339 on the local and deep-ocean forcing conditions, individual monthly heat flux transport ranges
340 from $4.79 \times 10^4 W / m^2$ (shoreward) in May 2004 to $-2.95 \times 10^4 W / m^2$ (seaward) in October 2004.
341 Further investigations of the seasonal trend of the total cross-shelf heat flux (not shown) indicate
342 the heat flux tends to be onshore during the winter and spring seasons and offshore during
343 summer and fall seasons.

344 The mean total salt flux is found to be shoreward at $6.67 \times 10^{-5} \pm 6.98 \times 10^{-4} Kg / m^2 s$.
345 Over the 4-year, the largest onshore flux ($0.0026 Kg / m^2 s$) occurred in May 2004, and the
346 largest offshore flux ($-0.0011 Kg / m^2 s$) occurred in October 2004. This model based mean salt
347 flux value is consistent with *Gawarkiewicz et al (2004)* with regards to its onshore transport
348 direction. However, the magnitude is smaller than earlier observational estimates (e.g.,
349 *Gawarkiewicz et al.; 2004; Garvine et al., 1988*), which were based on either single point
350 measurement or some limited ship transects for a short time period. Aside the temporal
351 averaging in our flux calculation may have smoothed the variability, differences in sampling
352 locations and durations between the model simulation and observations also contribute to the
353 magnitude difference.

354

355 ***C. Dominant Modes of shelfbreak jet***

356 While the focus in this study is on the mean state of MAB shelfbreak frontal circulation,
357 we can assess the dominant modes and temporal variability of the front and jet by applying the
358 Empirical Orthogonal Function (EOF) analysis on the simulated current fields along the
359 Nantucket transect. Because along-shelf and cross-shelf velocity fields are dynamically

360 connected, a bi-variant EOF method (*He et al.*, 2006) that concurrently considers both u and v
361 velocity components was adopted. Specifically, the data matrix A was defined as:

$$362 \quad A = \begin{pmatrix} u \\ v \end{pmatrix} \quad (6)$$

363 The EOF decomposition of A gives

$$364 \quad A(x, z, t) = \sum_{n=1}^N a_n(t) F_n(x, z) \quad (7)$$

365 where a_n and $F_n(x, z)$ are the temporal evolution functions and spatial eigenfunctions of each
366 EOF mode, respectively.

367 The first EOF mode accounts for 61% of variance (**Figure 12**). As expected, the along-
368 shelf velocity mode highlights the existence of the shelfbreak jet. The jet is located shoreward of
369 the shelfbreak. It is surface trapped with a characteristic width of about 20-30 km. The spatial
370 mode of the across-shelf velocity again reveals a layered vertical structure, which consists of a
371 shoreward flow in the interior and seaward flows in both surface and bottom boundary layers.
372 The principle component (PC1) of the 1st EOF mode is almost entirely positive, suggesting the
373 equator-ward shelfbreak jet and layer-structured cross-shelf flow patterns are persistent
374 shelfbreak circulation features. PC1 also reveals some short-duration flow reversals do occur
375 sporadically, which are presumably related to strong atmospheric forcing and frontal instability
376 (*Fratantoni and Pickart*, 2003). Overall, larger PC1 values occur during late winter and spring
377 seasons. Consistent with our early discussion (3.2.B), they imply the shelfbreak jet reaches its
378 maximum intensity during these times.

379 The second EOF mode accounts for 13% of total variance. Interestingly, this mode
380 displays contrasting flow patterns between the shelf and the slope in along-shelf direction. The
381 cross-shelf component is surface intensified and negative throughout the entire water column.

382 The 2nd principle component (PC2) suggests the mode is associated with significant temporal
383 variability that changes signs of spatial mode. Overall, this mode seems to be related to the
384 baroclinic eddy passages across the shelfbreak. The positive PC2 indicates cyclonic eddies
385 translating shoreward; whereas the negative PC2 corresponds to anticyclonic eddies translating
386 seaward. Generation of baroclinic eddies are subject to large-scale surface and deep-ocean
387 forcing conditions, and the flow interaction with the bottom topography. As such, no clear
388 seasonal trend is found in the PC2. With some 26% of the variance remaining in higher modes a
389 reconstruction of the shelfbreak circulation to account for its high frequency responses would
390 require several more modes.

391

392 **5. Summary**

393 A 1-km resolution model was developed to hindcast the MAB shelfbreak circulation from
394 December 2003 to June 2008. The model hindcast considered realistic atmospheric and tidal
395 forcing. The model's subtidal open boundary conditions were specified via one-way nesting with
396 an existing shelf-wide MABGOM circulation simulation by *He and Chen*, (submitted).
397 Hindcast solutions were compared with satellite altimeter data and hydrographic climatology for
398 the MAB shelfbreak. General agreements were found, indicating this shelfbreak circulation
399 model is capable of capturing essential dynamics of the MAB shelfbreak circulation. As we
400 focused on the mean structures of the shelfbreak current and hydrography in this study, time and
401 space continuous circulation hindcast fields from January, 2004 to December 2007 were used to
402 construct the temporal means and bimonthly averages of shelfbreak ocean states.

403 Our analysis showed that the MAB shelfbreak jet is a year-around, surface intensified
404 flow. On the average, it has characteristic width and trapping depth of 40 km and 100 m,

405 respectively, transporting 0.31 sv equator-ward. The jet reaches its maximum speed (0.3 ms^{-1}) in
406 the spring, when the shelfbreak temperature and salinity fronts fully develop. Throughout the
407 year, the bottom foot of the shelfbreak front migrates between 100m to 150m isobaths, reaching
408 its farthest offshore (onshore) position in April and May (November and December). The
409 accumulated temperature change (ATC) calculation within shelfbreak isopycnals suggests the
410 bottom boundary layer detachment is most significant during winter and spring seasons.

411 The relative vorticity analysis indicates the larger velocity shear exists seaward of the
412 shelfbreak, and that the vorticity ratio is roughly 2:1 between the seaward portion and shoreward
413 portion of the shelfbreak current. The geostrophy dominates the momentum balance of the
414 shelfbreak jet. The viscosity in the boundary layers and the nonlinear advection in the interior
415 play important roles in determining the ageostrophic flow. The cross-shelf volume transport, and
416 its associated heat and salt fluxes were estimated along the 200-m isobath within the model
417 domain. These values are characterized by small means with large standard deviations,
418 suggesting shelf/slope exchanges across the MAB shelfbreak are highly variable. Indeed, the
419 EOF analysis of the velocity fields along the Nantucket transect indicates that while the
420 shelfbreak jet is the dominant mode, the structure and intensity of the current are subject to
421 complex interactions between water stratification, wind forcing, baroclinic instabilities and
422 eddies. Further understandings of their roles controlling the shelfbreak circulation dynamics can
423 be achieved in the future by focused case studies using the high-resolution shelfbreak model
424 developed here. Clearly, deterministic predictions of the shelfbreak frontal circulation and its
425 associated material property transport between the shelf and deep-ocean will also require
426 advanced observational infrastructure together with sophisticated techniques for data
427 assimilation (e.g., *He et al.*, 2005; *He and Wilkin*, 2006). In that regard, the emerging MAB

428 shelfbreak pioneer array and new in-situ observations it is about to collect would be of great
429 importance.

430

431 **Acknowledgement**

432 We acknowledge research support provided through ONR grant N00014-06-1-0739 and NASA
433 grant NNX07AF62G. We are indebted to G. Gawarkiewicz, D. McGillicuddy for their valuable
434 discussions and suggestions throughout the course of this study.

435

436 **References**

437 Aikman, F., III, 1984: Pycnocline development and its consequences in the Middle
438 Atlantic Bight, *J. Geophys. Res.*, 89, 685-694.

439

440 Barth, J. A., D. Bogucki, S. D. Pierce, P. M. Kosro (1998), Secondary circulation associated with
441 a shelfbreak front, *Geophys. Res. Letts*, 25, 15, 2761-2764.

442

443 Beardsley, R. C., and C.N. Flagg, 1976: The water structure, mean currents, and shelf/slope
444 water front on the New England continental shelf, *Mem Soc. R. Sci. Liege*, 6(X), 209-225.

445

446 Beardsley, R. C., D. C. Chapman, K. H. Brink, S. R. Ramp, and R. Schlitz, 1985: The Nantucket
447 Shoals Flux Experiment (NSFE79). Part I: A basic description of the current and temperature
448 variability. *J. Phys. Oceanogr.*, 15, 713–748.

449

450 Burrage, D. M., and R. W. Garvine, 1988: Summertime hydrography at the shelfbreak front in
451 the Middle Atlantic Bight, *J. Phys. Oceanogr.*, 18, 1309-1319.

452

453 Chapman, D. C. and R. C. Beardsley, 1989: On the origin of shelf water in the Middle Atlantic
454 Bight. *Journal of Physical Oceanography*, 19, 384-391.

455

456 Chapman, D. C., and S. J. Lentz , 1994: Trapping of a coastal density front by the bottom
457 boundary layer, *J. Phys. Oceanogr.*, 24, 1464– 1479.

458

459 Chassignet, E. P., H. E. Hurlburt, O.M. Smedstad, G. R. Halliwell, P. J. Hogan, A. j. Wallcraft, R.
460 Baraille, and R. Bleck , 2006: The HYCOM (Hybrid Coordinate Ocean Model) data assimilative
461 system. *Journal of Marine Systems*, 65, 60-83.

462

463 Fairall, C. W., E. F. Bradley, J. E. Hare, A. A. Garchev, and J. Edson , 2003: Bulk
464 parameterization of air-sea fluxes: Updates and verification for the COARE algorithm. *Journal of*
465 *Climate*, 16, 571-591.

466

467 Flagg, C. N., R. W. Houghton, and L. J. Pietrafesa, 1994: Summertime thermocline salinity
468 maximum intrusions in the Middle Atlantic Bight, *Deep Sea Res., Part II* , 41, 325–340.

469

470 Flagg, C. N., M. Dunn,D. Wang, H. T. Rossby,R. L. Benway, 2006: A study of the currents of the
471 outer shelf and upper slope from a decade of shipboard ADCP observations in the Middle
472 Atlantic Bight, 111, C06003, doi:10.1029/2005JC003116.

473

474 Flather, R. A , 1976: A tidal model of the northwest European continental shelf, *Mem. Soc. R.*
475 *Sci. Liege*, 6(10),141-164.

476

477 Fratantoni, P. S., R. S. Pickart., D. J. Torres, A. Scotti, 2001: Mean Structure and Dynamics of
478 the Shelfbreak Jet in the Middle Atlantic Bight during Fall and Winter, *J. Phys. Oceanogr.*,
479 31,2135-2156.

480

481 Fratantoni, P.S., and R. S. Pickart, 2003: Variability of the shelf break jet in the Middle Atlantic
482 Bight: Internally or externally forced?, *Journal of Geophysical Research*, 108, NO. C5,
483 3166,doi:10.1029/2002JC001326.

484

485 Garvine, R., K. C. Wong, G. Gawarkiewicz, R. McCarthy, R. Houghton, and F. Aikman III (1988): The
485 morphology of shelf break eddies. *Journal of Geophysical Research*, 93, 15,593-15,607.

486 Gawarkiewicz, G. G., and D. C. Chapman, 1992: The role of stratification in the formation and
487 maintenance of shelf-break fronts, *J. Phys. Oceanogr.*, 22, 753–772..
488

489 Gawarkiewicz, G, F.Bahr, R.Bearsley, K.H.Brink, 2001: Interaction of a Slope Eddy with the
490 Shelfbreak Front in the Middle Atlantic Bight, *Journal of Physical Oceanography*,31,2783-2796.
491

492 Gawarkiewicz, G, K.H.Brink , R.Bearsley, M.Caruso, J.F.Lynch, C. Chiu, 2004: A large-
493 amplitude meander of the shelfbreak front during summer south of New England: Observations
494 from the Shelfbreak PRIMER experiment, *J. Geophys. Res.*,109,C03006,
495 doi:10.1029/2002JC001468.
496

497 He, R., McGillicuddy, D.J., Lynch, D.R., Smith, K.W., Stock, C.A., Manning, J.P., 2005. Data
498 assimilative hindcast of the Gulf of Maine coastal circulation. *Journal of Geophysical Research*,
499 110, C10011, doi:10.1029/2004JC002807.
500

501 He, R. and J. L. Wilkin, 2006: Barotropic tides on the southeast New England shelf: A view from
502 a hybrid data assimilative modeling approach, *Journal of Geophysical Research*, 111, C08002,
503 doi:10.1029/2005JC003254.
504

505 He, R. and R. H. Weisberg , 2002: West Florida shelf circulation and temperature budget for the
506 1999 spring transition, *Continental Shelf Research*, 22, 719-748.
507

508 He, R and K. Chen, Investigation of Northeastern North America Coastal Circulation Using a
509 Regional Circulation Hindcast Model, *Journal of Geophysical Research*, submitted
510 (http://omgrhe.meas.ncsu.edu/RHE/mabgom_09.pdf)
511

512 Houghton, R. W., R. Schlitz, R. C. Beardsley, B. Butman, and J. L. Chamberlin, 1982: The
513 Middle Atlantic Bight cold pool: Evolution of the temperature structure in summer 1979, *J.*
514 *Physc. Oceanogr.*, 12,1019-1029.

515 Houghton, R. W., F. Aikman III, H.W.Ou, 1988: Shelf-slope water frontal structure, and cross-
516 shelf exchange at the New England shelfbreak, *Cont.Shelf Res.*,8,687-710.
517

518 Houghton, R. W., C. N. Flagg, and L. J. Pietrafesa, 1994: Shelf-slope water frontal structure,
519 motion, and eddy heat flux in the southern Middle Atlantic Bight, *Deep Sea Res., Part II* ,
520 41, 273–306.
521

522 Lentz, S.J., 2008: Observations and a Model of the Mean Circulation over the Middle Atlantic
523 Bight Continental Shelf, *Journal of Physical Oceanography* ,38, 1203–1221.
524

525 Linder, C. A., and G. Gawarkiewicz, 1998: A climatology of the shelf break front in the Middle
526 Atlantic Bight, *J. Geophys. Res.*, 103, 18,405– 18,423.
527

528 Linder, Christopher A., G. G. Gawarkiewicz, and R. S. Pickart, 2004. Seasonal characteristics of
529 bottom boundary layer detachment at the shelfbreak front in the Middle Atlantic Bight. *Journal*
530 *of Geophysical Research*, VOL. 109, C03049, doi:10.1029/2003JC002032, 2004.
531

532 Loder, J. W., B. Petrie, and G. Gawarkiewicz, 1998: The coastal ocean off northeastern North
533 America: A large-scale view, in *The Sea*, Vol. 11, *The Global Coastal Ocean, Regional Studies*
534 *and Syntheses*, edited by A. R. Robinson and K. H. Brink, pp. 105-133, Wiley, New York.
535

536 Lozier, M. Susan, and Glen Gawarkiewicz, 2001. Cross-frontal exchange in the Middle Atlantic
537 Bight as evidenced by surface drifters. *Journal of Physical Oceanography*, **31**(8), Part 2, 2498-
538 2510.
539

540 Lozier, S., M. Reed and G. Gawarkiewicz, 2002. Linear stability of shelfbreak fronts. *Journal of*
541 *Physical Oceanography*, 32(3), 924-944.
542

543 Luetlich, R. A., J. J. Westerink, and N. W. Scheffner, 1992: ADCIRC: An advanced three-
544 dimensional circulation model for shelves, coasts, and estuaries. U.S. Army Engineer Waterways
545 Experiment Station.

546 Manning, J., 1991: Middle Atlantic Bight salinity: Interannual variability, *Cont. Shelf Res.*, 11,
547 123-137.

548

549 Marchesiello, P. J. C. McWilliams, and A. Shchepetkin, 2003: Equilibrium structure and
550 dynamics of the California current system. *Journal of Physical Oceanography*, 33, 753-783.
551

552 Marchesiello, P., J. C. McWilliams, and A. F. Shchepetkin, 2001: Open boundary conditions for
553 long-term integration of regional oceanic models. *Ocean Modelling*, 3, 1-20.

554

555 Marra, J., R. W. Houghton, D.C. Boardman, and P. J. Neale, 1982: Variability in surface
556 chlorophyll a at a shelf-break front, *J. Mar. Res.*, 40, 575-591.

557

558 Marra, J., R. W. Houghton, and C. Garside, 1990: Phytoplankton growth at the shelf-break front
559 in the Middle Atlantic Bight, *J. Mar. Res.*, 48, 851-868.

560

561 Mellor, G. L. and T. Yamada , 1982: Development of a turbulence closure model for geophysical
562 fluid problems. *Review of Geophysics*, 20, 851-875..

563

564 Pickart, R., D. Torres, T. McKee, M. Caruso, and J. Przystup , 1999: Diagnosing a meander of
565 the shelfbreak front in the Middle Atlantic Bight, *J. Geophys. Res.*, 104, 3121–3132.

566

567 Pickart, R. S., 2000: Bottom boundary layer structure and detachment in the shelfbreak jet of the
568 Middle Atlantic Bight, *J. Phys. Oceanogr.*, 30, 2668– 2686.

569

570 Rio, M. H. and F. Hernandez, 2004: A mean dynamic topography computed over the world ocean
571 from altimetry, in-situ measurements, and a geoid model, *Journal of Geophysical Research*, 109,
572 c12032, doi: 10.1029/2003JC002226.

573

574 Ryan, J.P, J.A.Yorder, J.A.Bath, P.C. Cornillon. 1999: Chlorophyll enhancement and mixing
575 associated with meanders of the shelf break front in the Mid-Atlantic Bight. J. Geophys. Res.,
576 104(C10), 23,479–23,493.

577

578 Ryan, J.P., J. A. Yoder, and P.C. Cornillon, 1999: Enhanced chlorophyll at the shelfbreak of the
579 Mid-Atlantic Bight and Georges Bank during the spring transition. Limnol. Oceanogr., 44(1), 1-
580 11.

581

582 Shchepetkin, A.F., and J.C., McWilliams, 2005: The regional oceanic modeling system (ROMS):
583 a split-explicit, free-surface, topography-following-coordinate oceanic model. Ocean Modelling,
584 9, 347-404.

585

586

587 Figure Captions

588

589 Figure1. The high resolution shelfbreak model domain (pink box) and the location of Nantucket transect
590 discussed in the manuscript (red line). Also shown is the satellite track (black line), along which the sea
591 surface height anomaly data were sampled. The blue dots along the highlighted 200-m isobath and their
592 associated numbers indicate the along-isobath distance downstream from the model's northeastern boundary.

593

594 Figure 2. Hovmoller diagrams of satellite observed and model simulated sea surface height anomaly (SSHA)
595 along the cross-shelf transect for the period from January 2004 to December 2007.

596

597 Figure3. The bi-monthly mean temperature transect comparison between the model solutions (left panels) and
598 the climatology (right panels) of *Linder and Gawarkiewicz (1998)*.

599

600 Figure4. The bi-monthly mean salinity transects comparison between the model solutions (left panels) and the
601 climatology (right panels) of *Linder and Gawarkiewicz (1998)*.

602

603 Figure 5. Model simulated mean temperature, salinity, along-shelf velocity and cross-shelf velocity fields
604 along the Nantucket transect.

605

606 Figure 6. Simulated bi-monthly mean along-shelf velocity fields and their associated net equator-ward
607 transport.

608

609 Figure 7. Bi-monthly Accumulated Theta Change (ATC) fields along the Nantucket transect. The ATC
610 calculation is based on modeled bi-monthly density fields. The purple lines are the isopycnals, and the
611 color shading stands for the intensity of ATC. The upward tilted, low-value ATC is an indication

612 of the BBL convergence and detachment.

613

614 Figure 8. Monthly migrations of the shelfbreak frontal foot (left) and the histogram showing the corresponding
615 depth of the frontal foot in each month.

616

617 Figure 9. The comparison between simulated (left) and observed (right, adopted from *Fratantoni et al.*, 2001)
618 mean vorticity fields at the shelfbreak. Both fields are scaled by the local Coriolis parameter.

619

620 Figure10. The mean cross-shelf momentum balance. From top to bottom and left to right are the Coriolis force,
621 the Pressure Gradient force (PGF), the residual of Coriolis plus PGF terms (i.e., ageostrophic term), the
622 viscosity term, the residual of ageostrophic term plus viscosity, the nonlinear advection term, the residual of
623 ageostrophic plus viscosity and advection terms, and the local rate of change term.

624

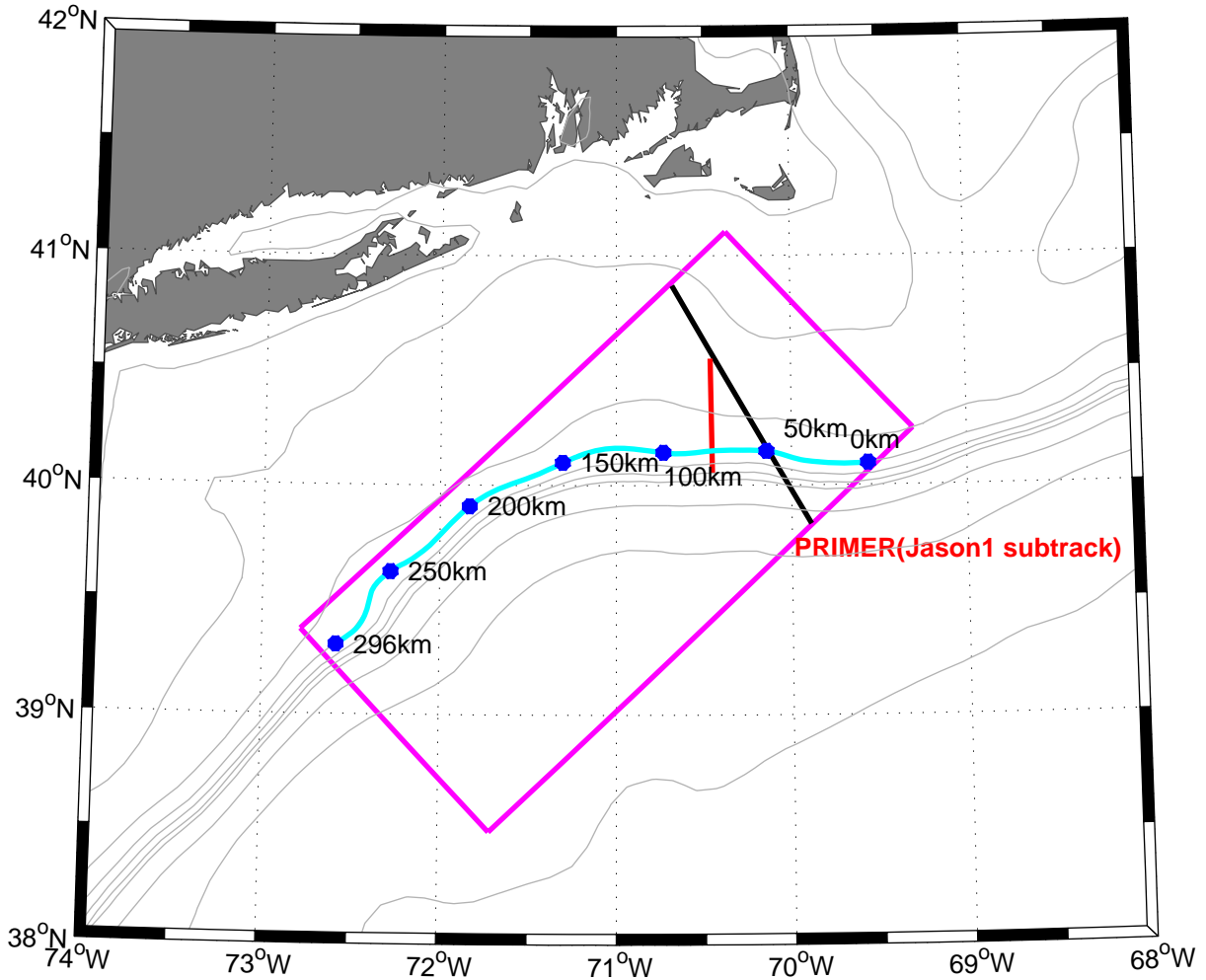
625 Figure 11. The cross-shelf volume transport along the 200m isobath inside the shelfbreak ROMS domain. The
626 x-axis is the along-isobath distance starts from zero (off the Nantucket shoal) to 300-km (off the Hudson
627 Canyon).

628

629 Figure 12 The first two EOF modes of simulated shelf break circulation, and their corresponding principle
630 components. U (V) is the alongshore (cross-shelf) velocity component along the Nantucket transect.

631

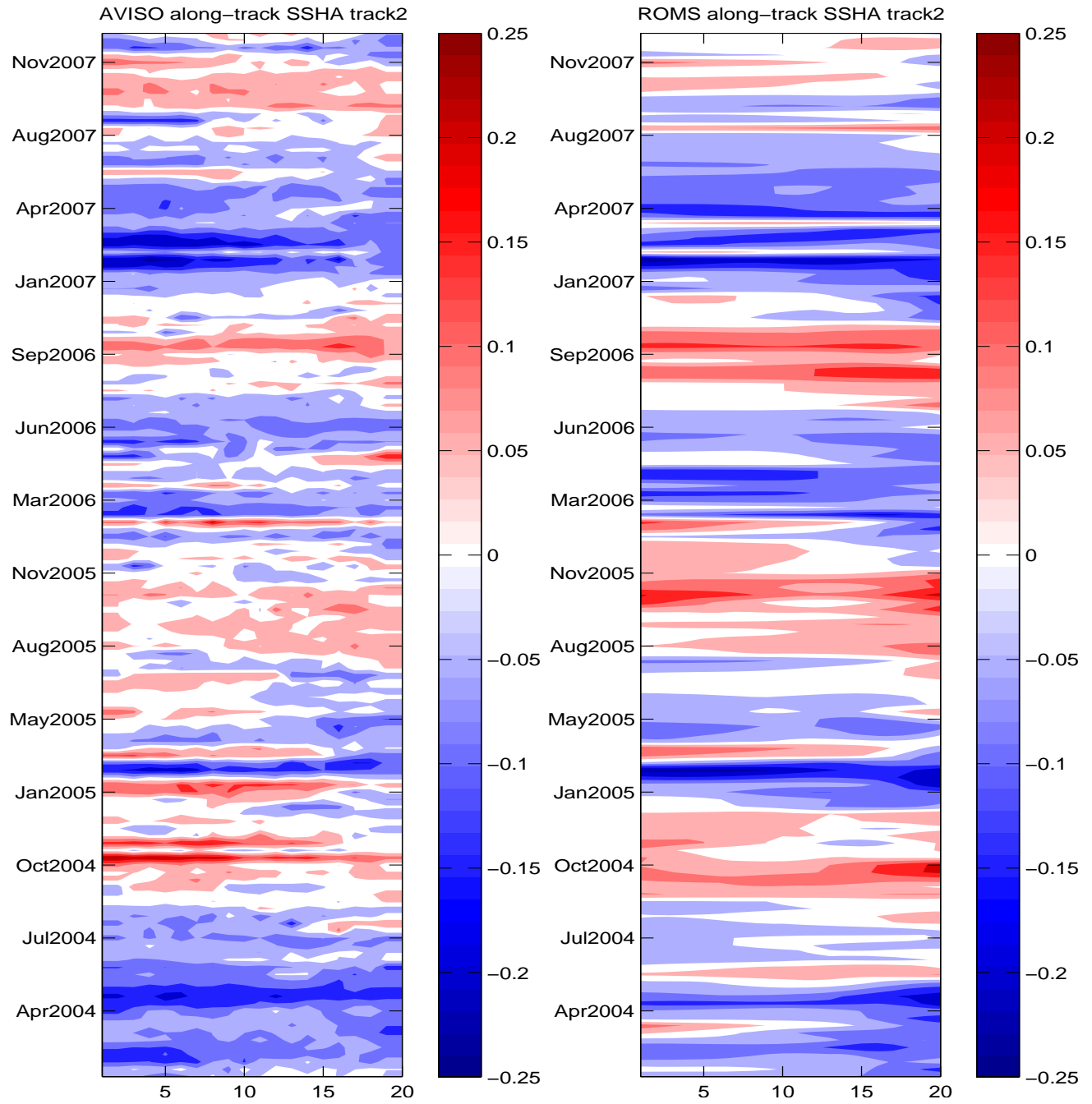
632



633

634 Figure1. The high resolution shelfbreak model domain (pink box) and the location of Nantucket transect
635 discussed in the manuscript (red line). Also shown is the satellite track (black line), along which the sea
636 surface height anomaly data were sampled. The blue dots along the highlighted 200-m isobath and their
637 associated numbers indicate the along-isobath distance downstream from the model's northeastern boundary.

638



639

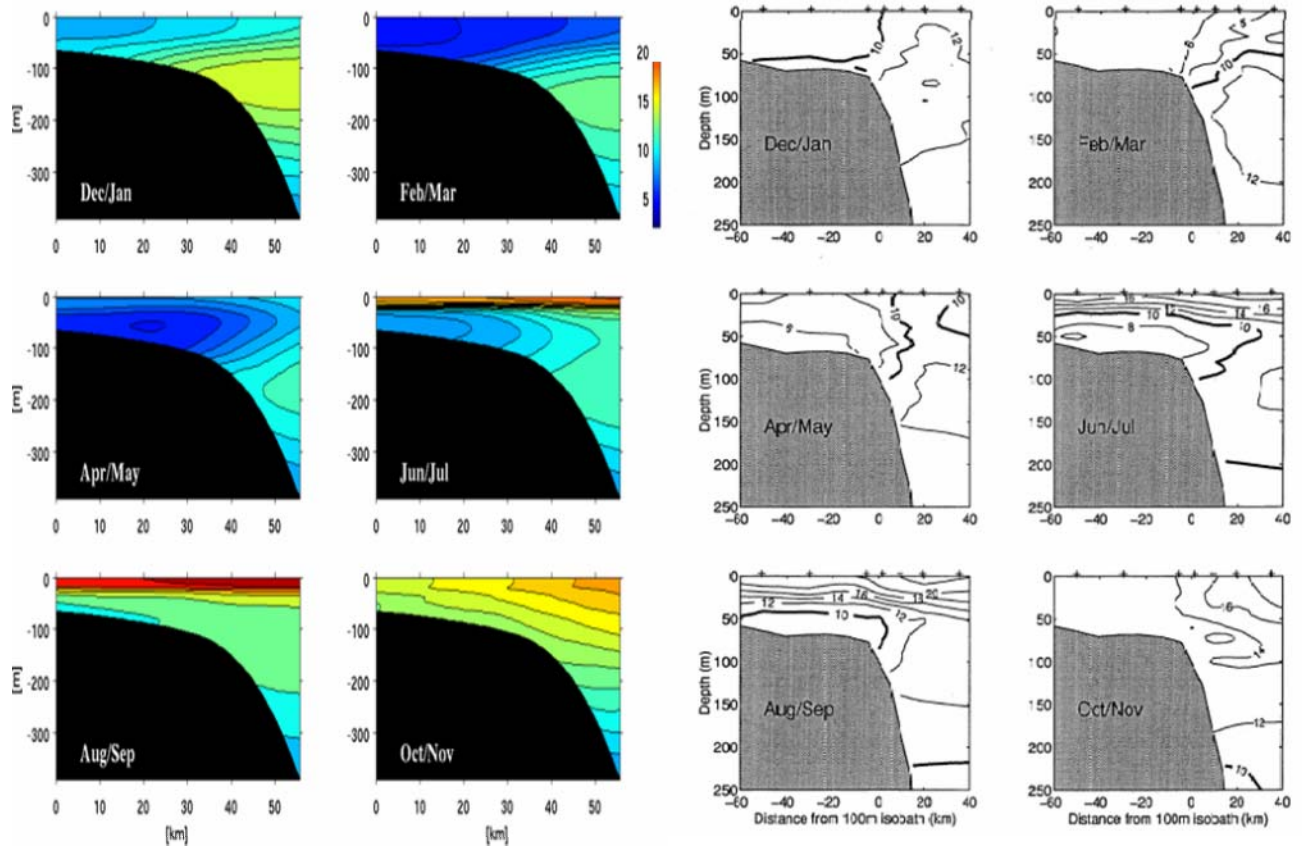
640 Figure 2. Hovmoller diagrams of satellite observed and model simulated sea surface height anomaly (SSHA)

641 along the cross-shelf transect for the period from January 2004 to December 2007.

642

643

644



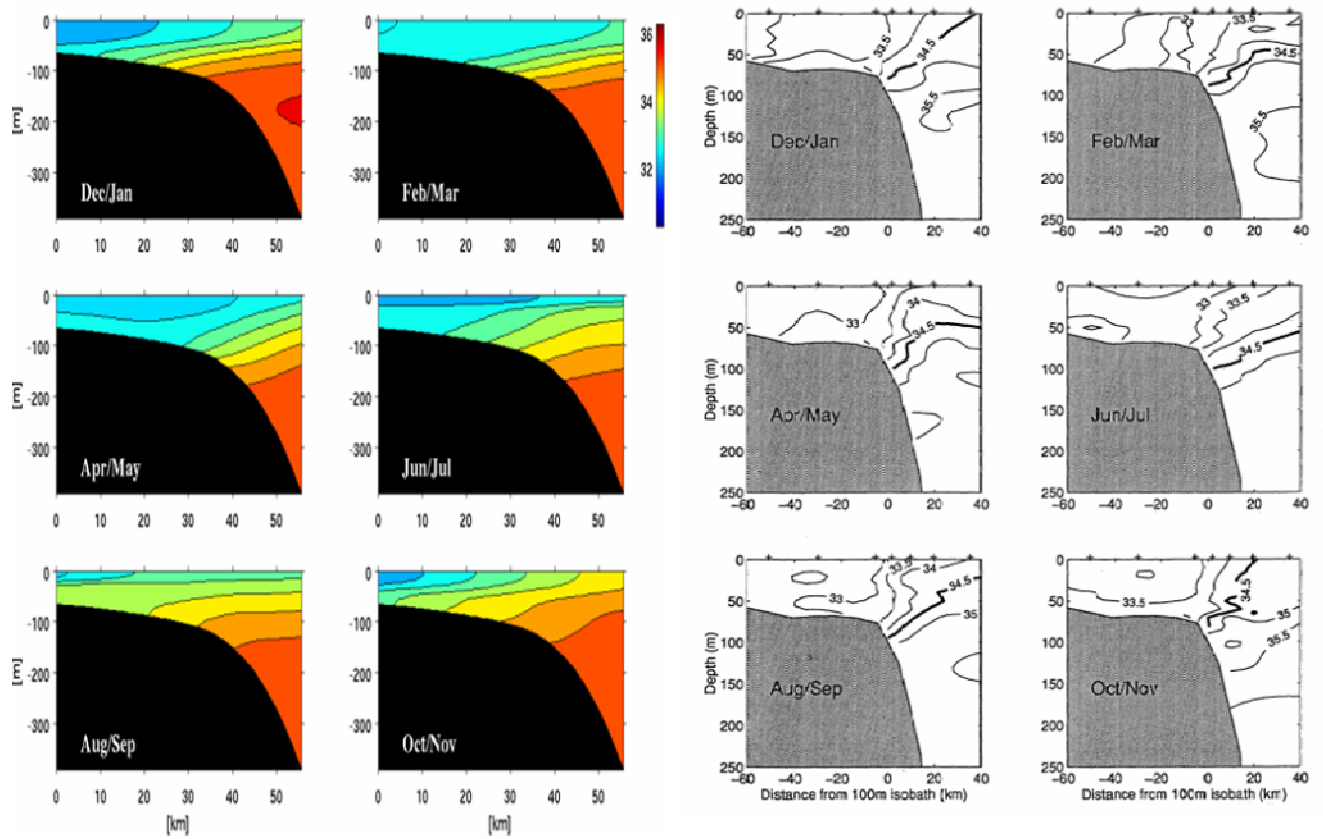
645

646

647 Figure3. The bi-monthly mean temperature transect comparison between the model solutions (left panels) and

648 the climatology (right panels) of *Linder and Gawarkiewicz (1998)*.

649



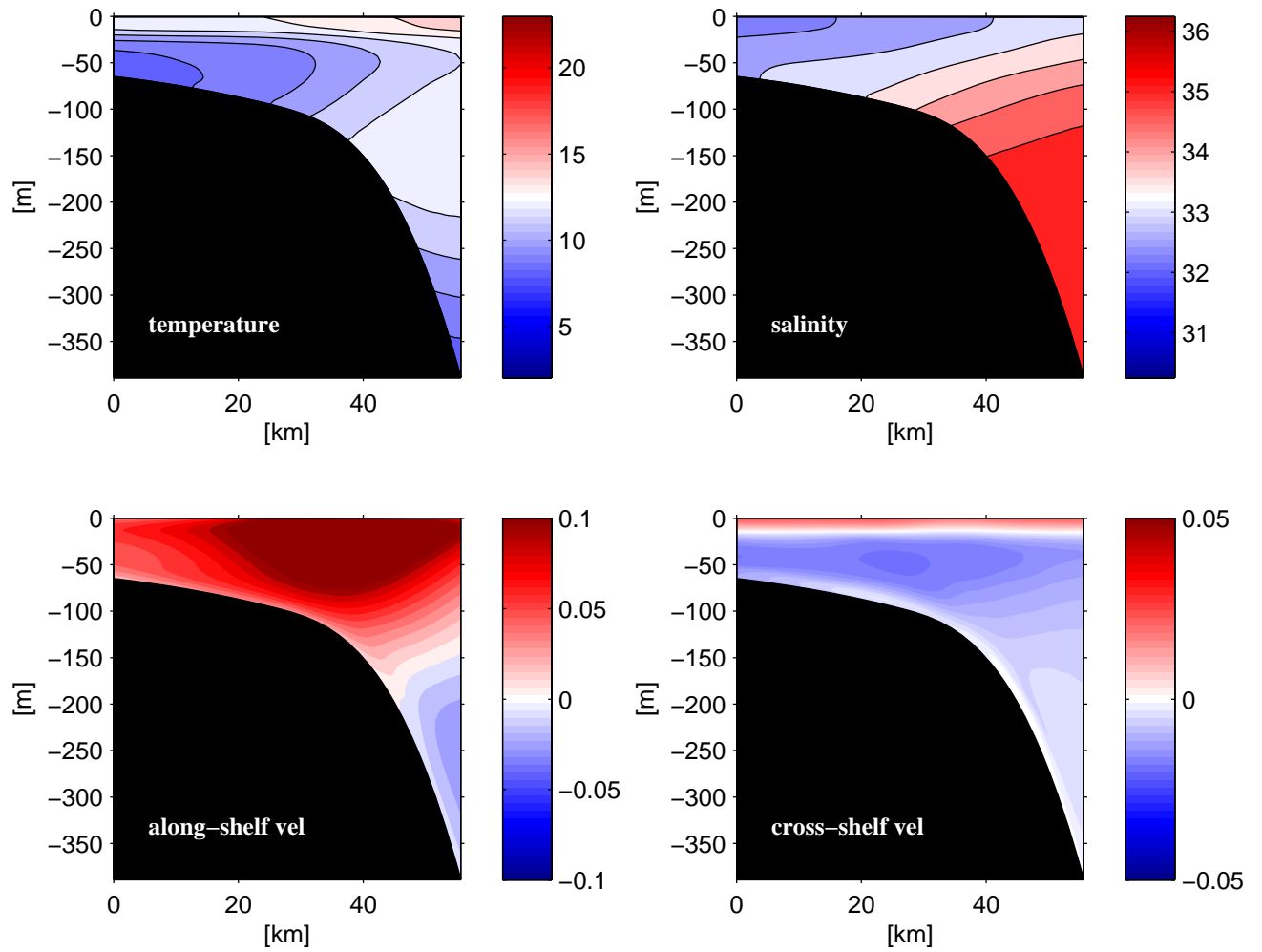
650

651

652 Figure4. The bi-monthly mean salinity transects comparison between the model solutions (left panels) and the
 653 climatology (right panels) of *Linder and Gawarkiewicz (1998)*.

654

655



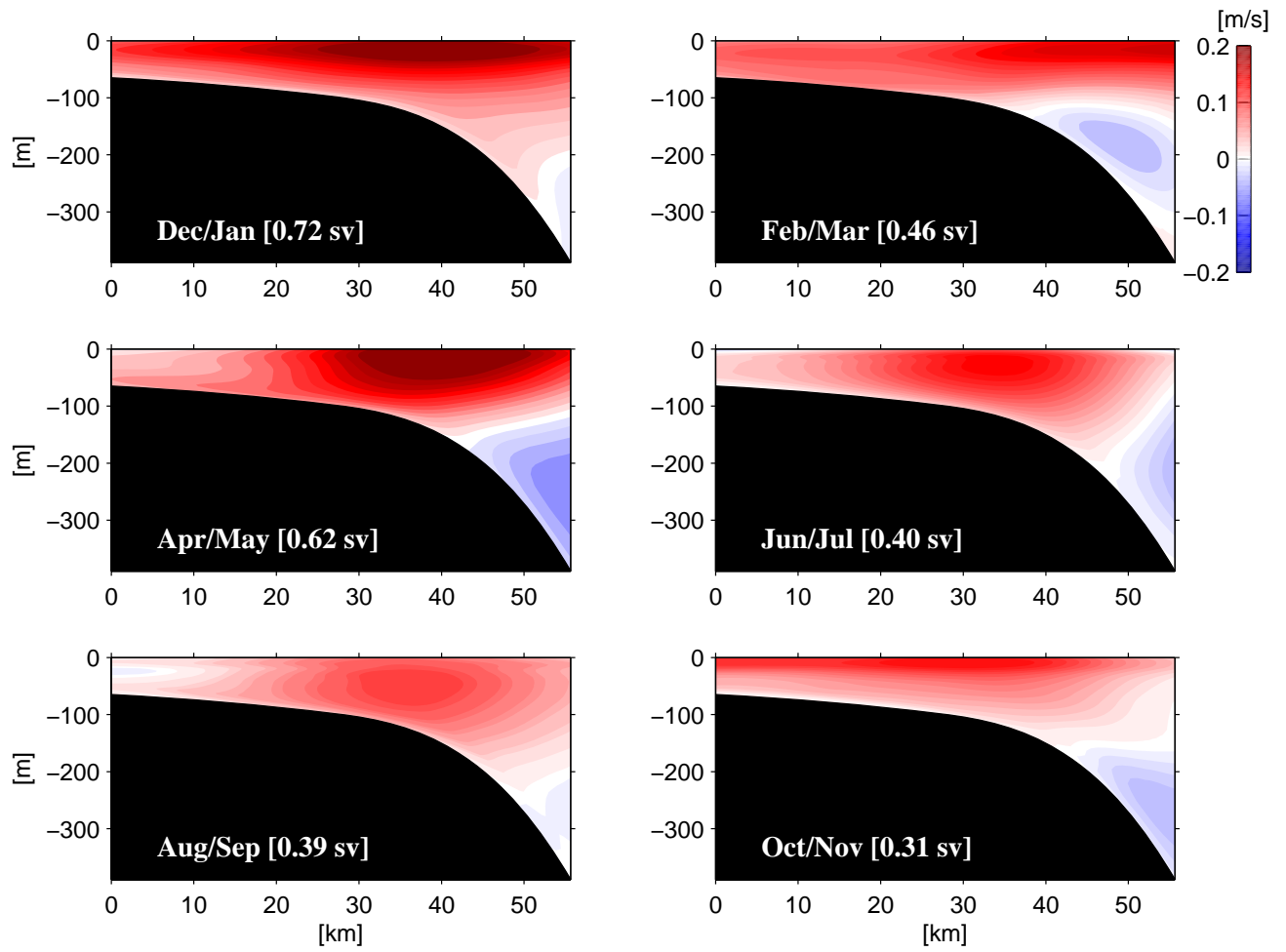
656

657

658 Figure 5. Model simulated mean temperature, salinity, along-shelf velocity and cross-shelf velocity fields

659 along the Nantucket transect.

660

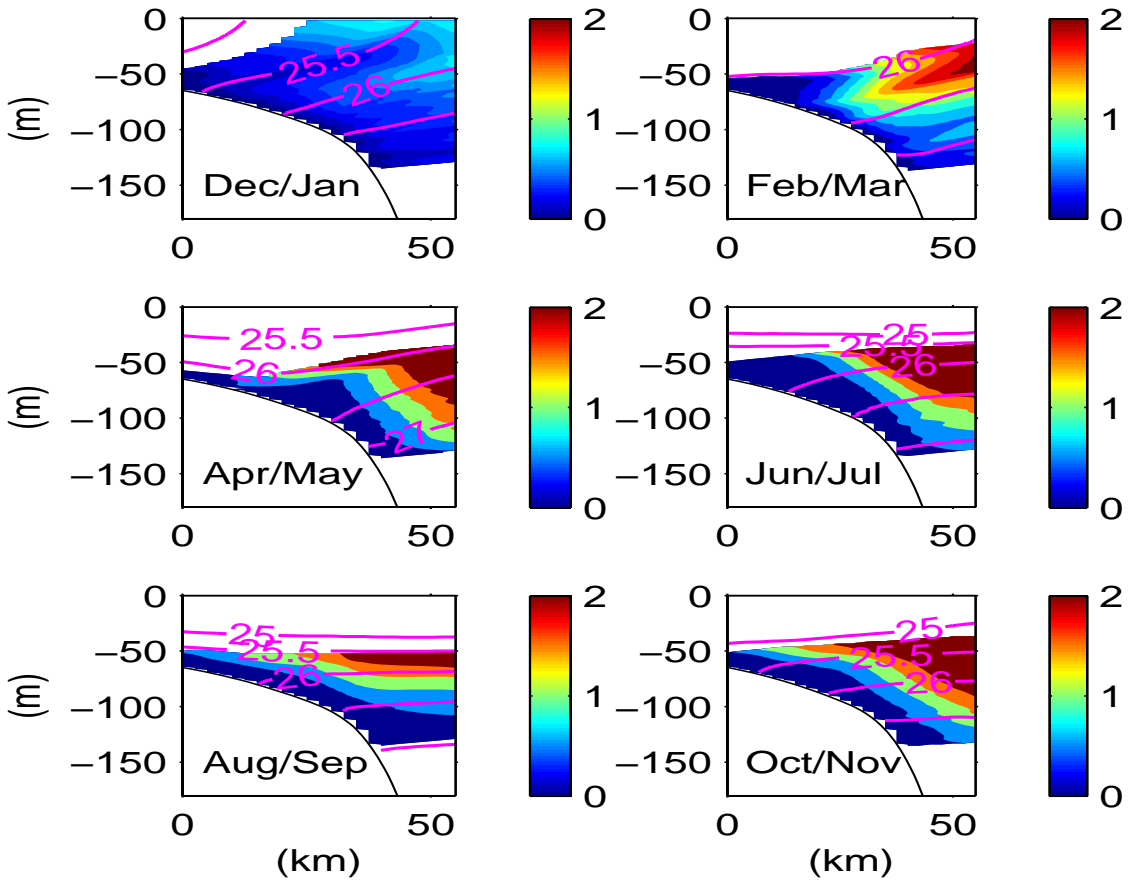


661

662 Figure 6. Simulated bi-monthly mean along-shelf velocity fields and their associated net equator-ward

663 transport.

664



665

666

Figure 7. Bi-monthly Accumulated Theta Change (ATC) fields along the Nantucket transect. The ATC

667

calculation is based on modeled bi-monthly density fields. The purple lines are the isopycnals, and the

668

color shading stands for the intensity of ATC. The upward tilted, low-value ATC is an indication

669

of the BBL convergence and detachment.

670

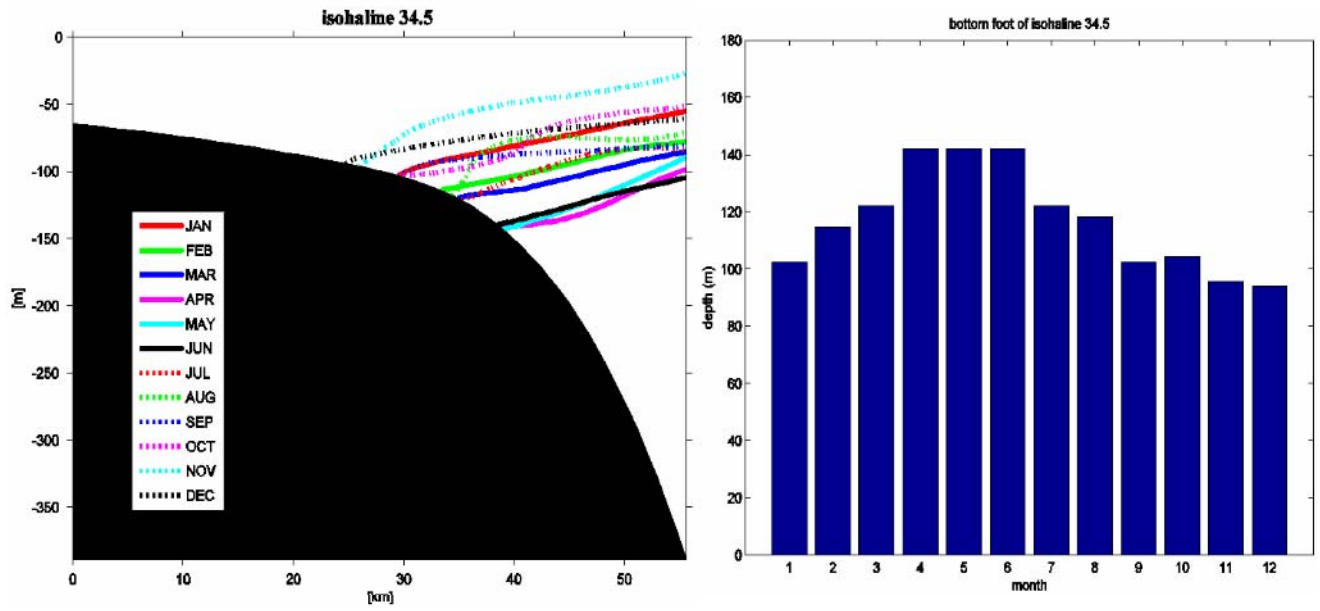
671

672

673

674

675



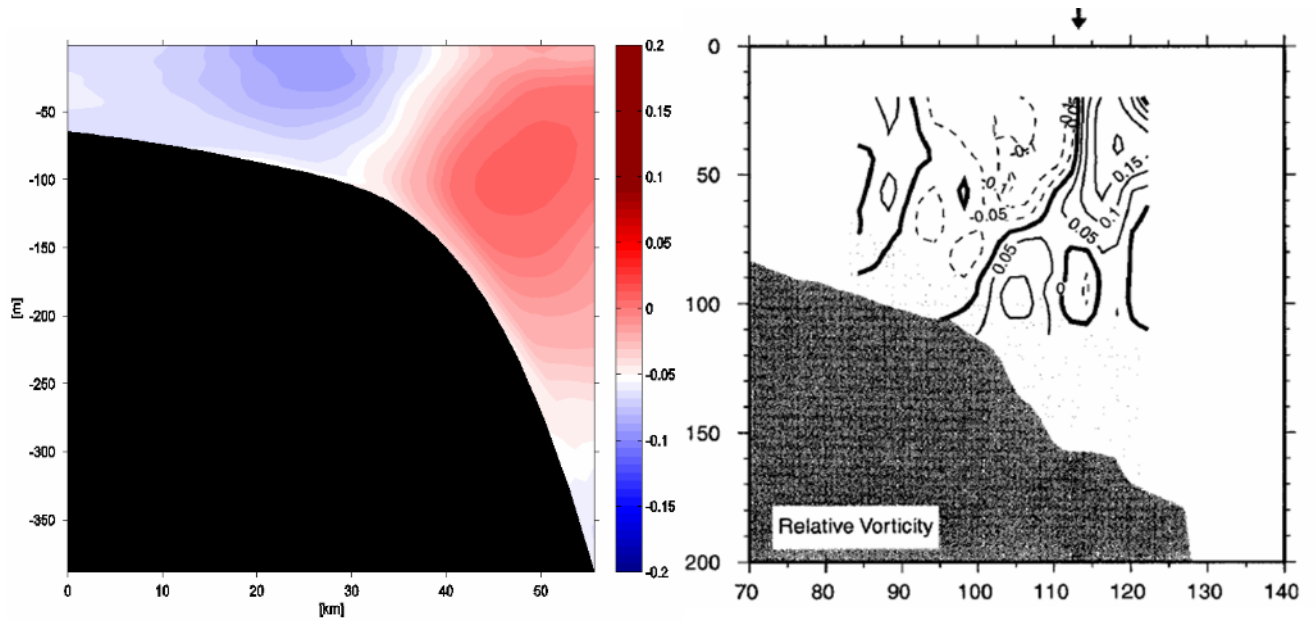
676

677 Figure 8. Monthly migrations of the shelfbreak frontal foot (left) and the histogram showing the corresponding

678 depth of the frontal foot in each month.

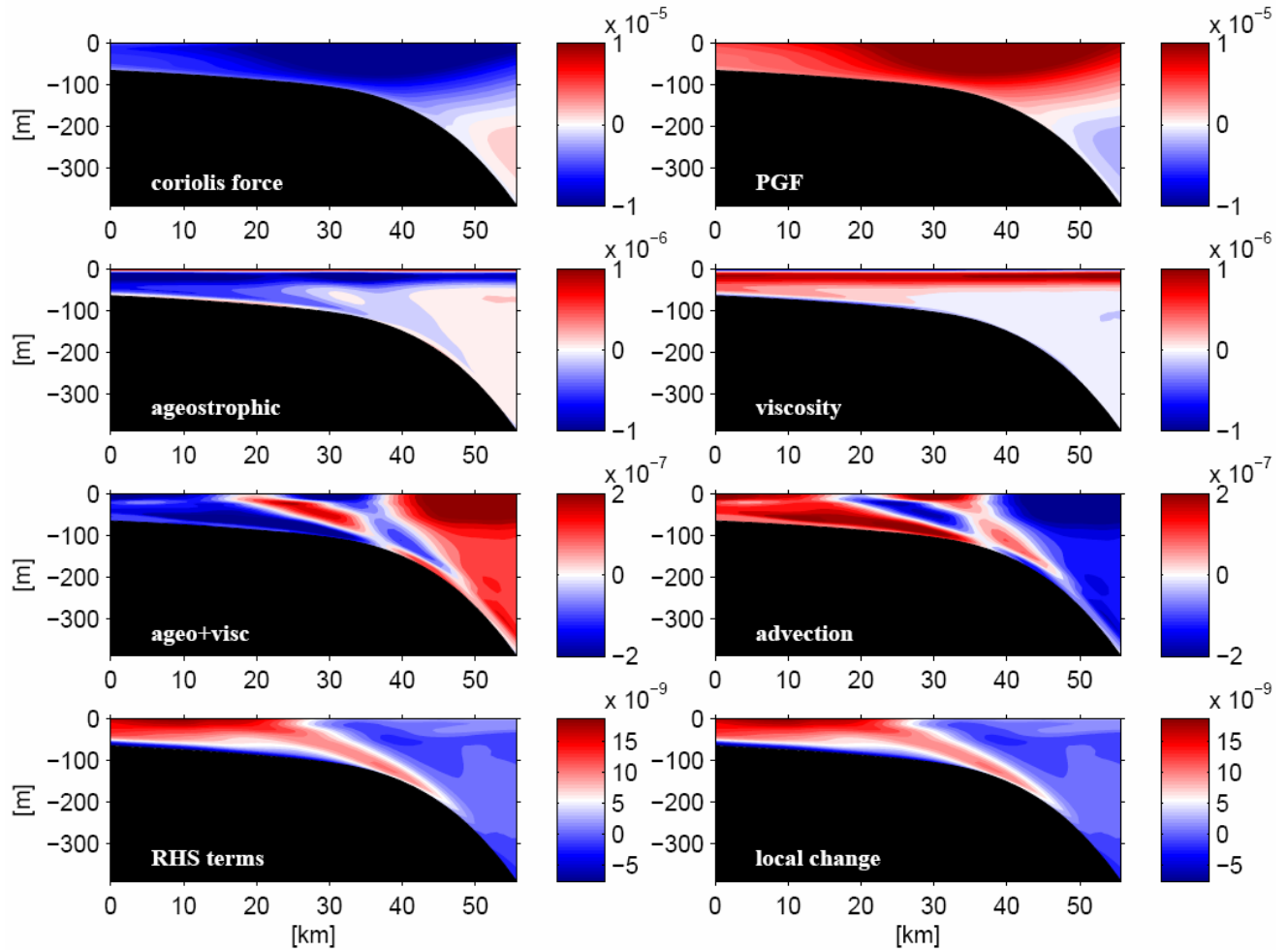
679

680
681
682



683
684
685
686

Figure 9. The comparison between simulated (left) and observed (right, adopted from *Fratantoni et al., 2001*) mean vorticity fields at the shelfbreak. Both fields are scaled by the local Coriolis parameter.



687

688

689 Figure10. The mean cross-shelf momentum balance. From top to bottom and left to right are the Coriolis force,

690 the Pressure Gradient force (PGF), the residual of Coriolis plus PGF terms (i.e., ageostrophic term), the

691 viscosity term, the residual of ageostrophic term plus viscosity, the nonlinear advection term, the residual of

692 ageostrophic plus viscosity and advection terms, and the local rate of change term.

693

694

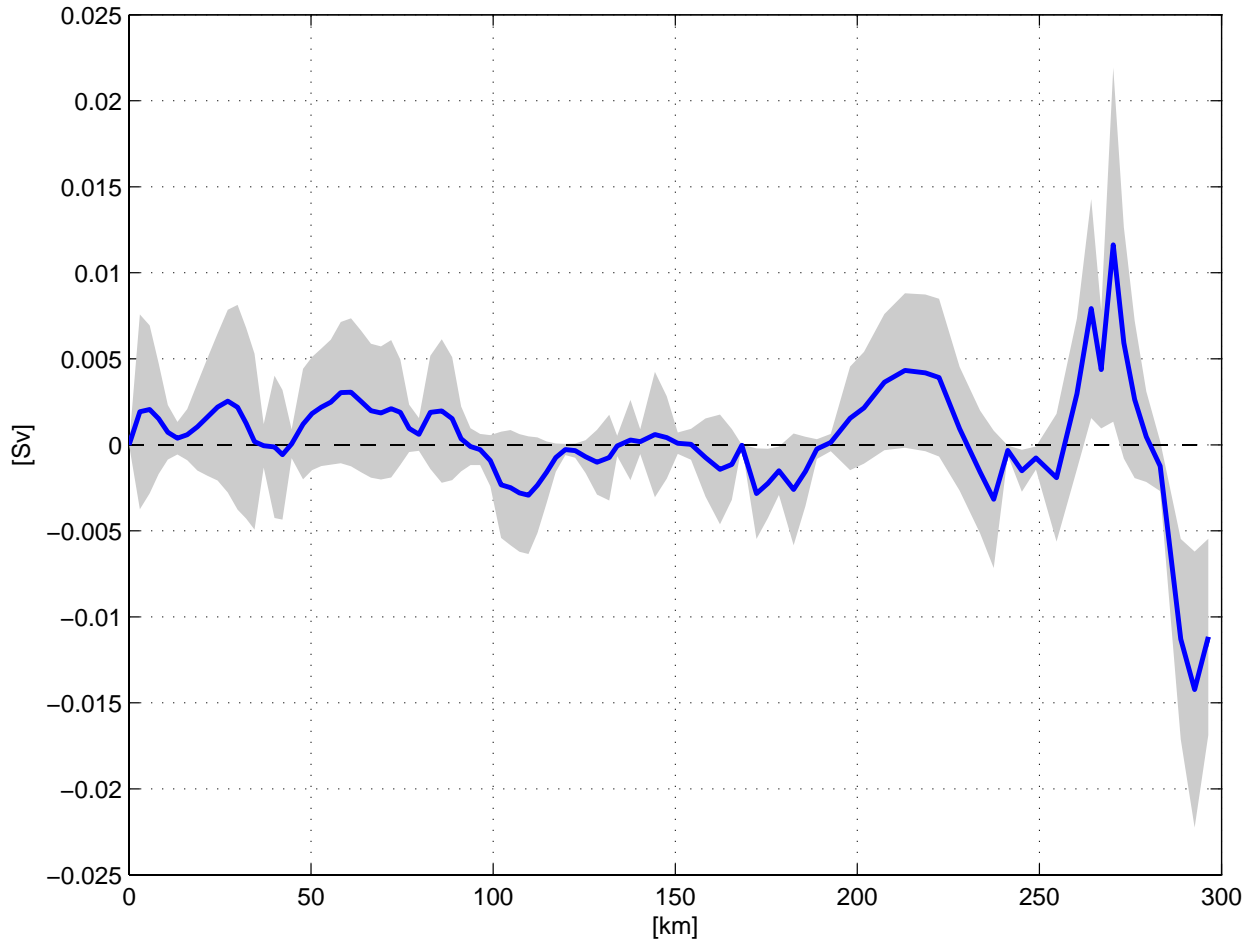
695

696

697

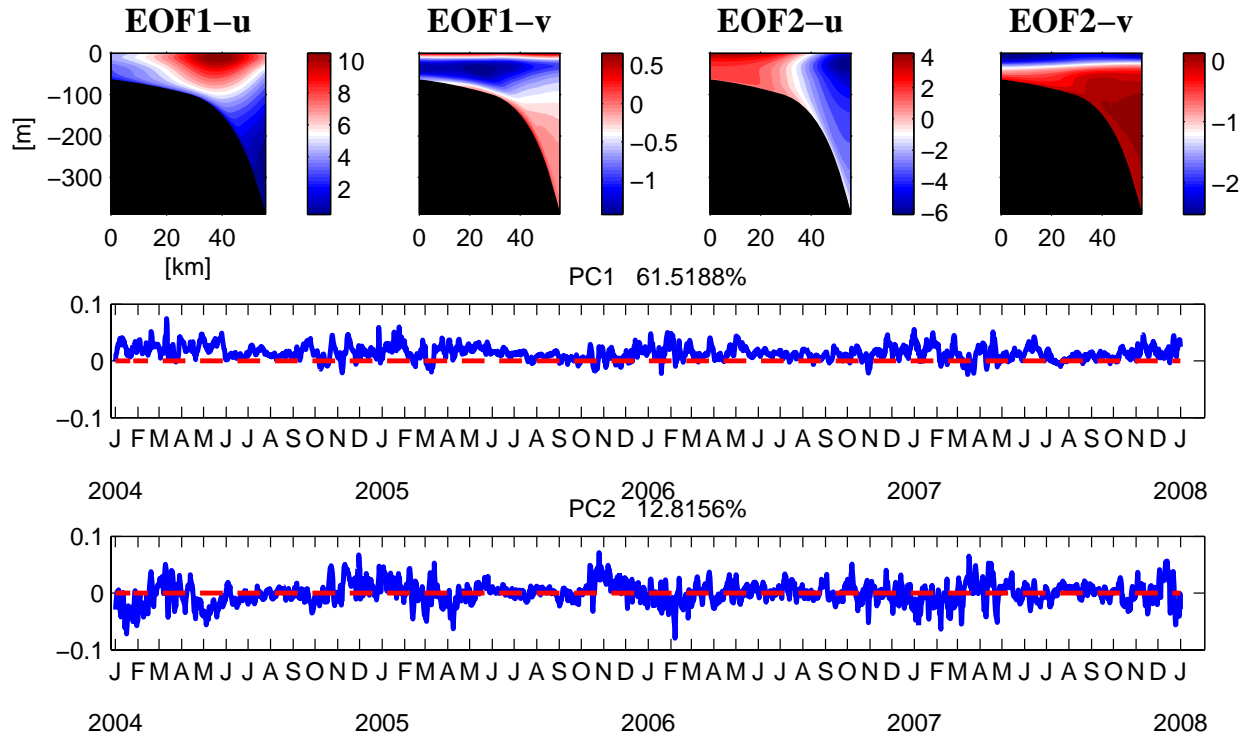
698

699
700
701



702
703
704
705

Figure 11. The cross-shelf volume transport along the 200m isobath inside the shelfbreak ROMS domain. The x-axis is the along-isobath distance starts from zero (off the Nantucket shoal) to 300-km (off the Hudson Canyon).



706

707 Figure 12 The first two EOF modes of simulated shelf break circulation, and their corresponding principle

708 components. U (V) is the alongshore (cross-shelf) velocity component along the Nantucket transect.

709

710